What Role Does the Barrier Layer Play During Extreme El Niño Events?

Xiaolin Zhang[1] , Janet Sprintall[2] , and Lili Zeng[3,4]

[1]Oceanography Remote Sensing & Assimilation, University of Hamburg, Hamburg, Germany, [2]Scripps Institution of Oceanography, La Jolla, CA, USA, [3]Southern Marine Science and Engineering Guangdong Laboratory (Guangzhou), Guangzhou, China, [4]State Key Laboratory of Tropical Oceanography, South China Sea Institute of Oceanology, Chinese Academy of Sciences, Guangzhou, China

Abstract Intensive air-sea interaction and the formation of the salinity barrier layer (BL) in the Pacific has fundamental importance to the El Niño evolution. The structure and formation of the BL in the equatorial Pacific Ocean during moderate and extreme El Niños over the past 30 years are investigated using in situ temperature and salinity data measured by the TAO/TRITON array and the data-assimilating ECCO2 product. In the western and central Pacific Ocean, the BL is thicker during moderate El Niños compared to extreme El Niños due to a deeper isothermal layer depth compared to the density defined mixed layer depth. Moreover, in the western and central Pacific Ocean, the anomalous zonal eastward current related to the westerly wind event that initiates El Niños is found to be stronger during extreme El Niños, advecting the thicker BLs from west to east. A salinity budget suggests that during both moderate and extreme El Niño events, surface freshwater flux dominates at the equator. During extreme El Niños, the change in the freshwater flux drives a strong surface jet in the far western Pacific at 1°S, 156°E. North of the equator, the surface freshwater flux largely dampens this advective impact. Thus during the different El Niño strengths, the BL distribution, evolution and impact are also different. This suggests that climate models need to better distinguish different types of El Niño events in order to simulate the ENSO dynamics correctly.

Plain Language Summary During the different El Niño scenarios, the barrier layer (BL) distribution, evolution and impact are different. Observations from TAO/TRITON array shows that the BL is thicker during moderate El Niños than during extreme El Niños in the western and central Pacific Ocean. Less heat input leads to a thinner isothermal layer depth during extreme El Niños. Stronger anomalous zonal eastward current during extreme El Niños advects the thicker BLs from west to east, dampens thick BL maintaining in the western and central Pacific Ocean. During extreme El Niños, the diagnosis shows that the change in the freshwater flux further drives a strong eastward surface jet mainly through salinity effect in the far western Pacific, further advect the thick BL to the east. Climate models need to better distinguish the evolution of BL during different types of El Niño events.

1. Introduction

In most regions of the ocean, the mixed layer depth (MLD) determined by the density stratification is the same as the isothermal layer depth (ILD). However, when the ILD is deeper than the MLD, a "barrier layer" (BL) exists (Lukas & Lindstrom, 1991) that can inhibit the vertical mixing of cold water from below into the mixed layer (Godfrey & Lindstrom, 1989) as well as trap the incoming solar radiation to a shallower surface layer. BLs can form for a variety of reasons: as a result of heavy rainfall, especially (but not only) under light wind conditions; the horizontal advection of a remotely formed BL; the tilting of near-vertical salinity contours due to vertical shear in horizontal currents; and the vertical stretching of the upper water column, assuming the pre-existence of a BL (Bosc et al., 2009; Cronin & McPhaden, 2002; Vialard & Delecluse, 1998). River runoff, subduction of high salinity waters, the deepening of the ILD and mesoscale eddy processes and down-welling propagating waves can also impact BL formation and evolution (Foltz & McPhaden, 2009; Girishkumar et al., 2011; Mignot et al., 2009; Parampil et al., 2010; Thadathil et al. 2007, 2008; Zeng et al., 2009; Zeng & Wang, 2017).
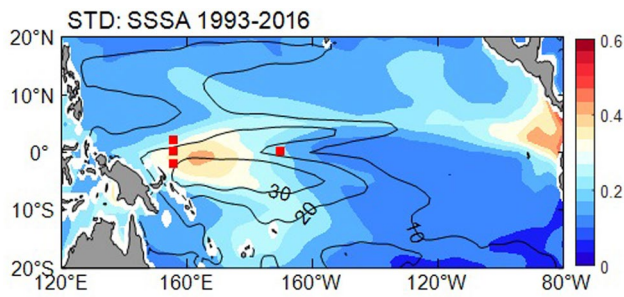
Figure 1. Standard deviation of monthly sea surface salinity anomaly (color shading) and mean BL thickness (contours, units: m) based on the ECCO2 output for the period of 1993–2016. The red squares denote the four TAO\TRITON mooring stations used for this study. BL, barrier layer; ECCO2, Estimating the Circulation and Climate of the Ocean.

Previous theories have suggested a fundamental influence of the vertical salinity stratification on the heat buildup for the maintenance of the warm pool (Maes et al., 2002) and the evolution of El Niño events (Cronin & McPhaden, 2002; Maes et al. 2002, 2005). During El Niño events there is intense air-sea interaction and heavy rainfall over the warm sea surface in the central Pacific Ocean, and the formation of salinity-stratified BLs can help sustain the higher surface temperature by inhibiting the vertical transfer of heat. Cai et al. (2014) showed that compared to moderate El Niño events, extreme El Niño events are characterized by a massive reorganization of atmospheric convection in the tropical Pacific Ocean and extension of the warm pool edge into the eastern Pacific (See Figure 1 from Cai et al., 2014). More specifically, during extreme El Niños, rainfall not only increases tremendously in the central Pacific Ocean but that rainfall can also extend further into the eastern equatorial Pacific. This might suggest that the presence of thicker BLs is more extensive throughout the Pacific due to the stronger rainfall experienced during extreme El Niños. However contrary to expectations, our study will show that in the western and central Pacific Ocean, thinner BLs occur during extreme El Niños compared to moderate El Niño events. This means that other processes must also play an important role in BL formation during these two El Niño strengths.

In this study, we estimate the spatial distribution of the BL during moderate and extreme El Niño events since the 1990s, and explore the related mechanisms responsible for the BL formation. Previous studies have shown that a "freshwater jet" forms in the western Pacific Ocean in response to the presence of BLs (Roemmich et al., 1994; Zhang & Clarke, 2015). We examine the role of this jet on the dynamics occurring during the two different El Niño strengths.

The overall structure of the study is as follows. The data sets and methodology are described in Section 2. Major features of the upper ocean stratification are presented in Section 3. Section 4 compares the BL thickness during the moderate and extreme El Niños. The oceanic and atmospheric conditions under each El Niño strength are examined in Section 5 and a salinity budget is performed in Section 6 with a focus on the formation mechanisms of the BL. Dynamics of the freshwater jet in the western Pacific Ocean formed in response to the BL under extreme and moderate El Niños is discussed in Section 7. Section 8 discusses and summarizes the main results.
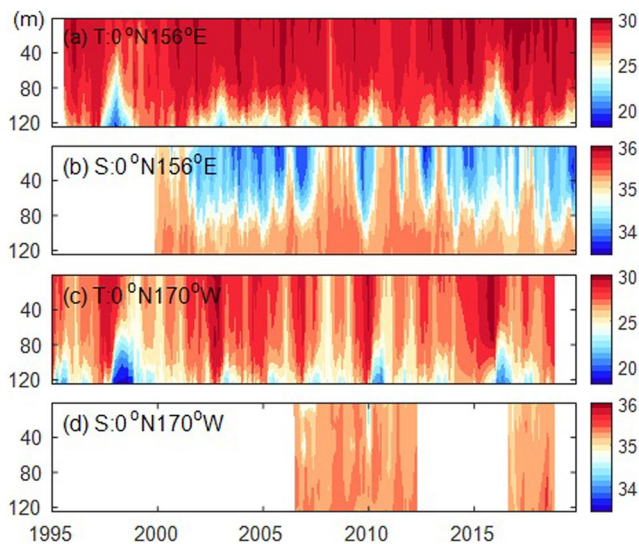
2. Data Sets and Methodology

2.1. Data Sets

Monthly in situ temperature and salinity data from the TAO/TRITON moored array at 0°, 156°E and 0°, 170°W, that have records covering the period 1995 through 2016 (Figure 1), are used to explore the upper ocean stratification. These two TAO stations that are the focus of our study represent the western Pacific Ocean warm pool region (0°, 156°E) and the central Pacific Ocean (0°, 170°W) (Figure 2) as we expect that there will be significant change in the BLT in each of these regions. In addition, these two sites have a more complete time series of TAO salinity data needed to determine the density-defined MLD. There are very few salinity data available with depth from the TAO array in the eastern Pacific Ocean. Additional temperature and salinity data at 2°S, 156°E and 2°N, 156°E were used to estimate the "freshwater" jet.

The available salinity records were typically measured at the surface (1–3 m), then roughly every 5–10 m to 30 m depth and every 20–25 m down to 300 m. Temperature sensors were similarly distributed along the mooring line. However, data were not always available at each depth.

Figure 2. Time evolution of the upper 125 m *in situ* (a) temperature (°C) and (b) salinity at 0°, 156°E based on TAO/TRITON data. Panels (c and d) are the same but for 0°, 170°W.

Hence in order to make a complete vertical profile, the salinity and temperature data were vertically decimated to depth levels of 1 m, then 25 m intervals between 25–150 m depth and 50 m intervals between 150–300 m. Occasional temporal gaps at discrete depths were filled using a weighted linear interpolation approach.

The monthly gridded temperature and salinity data (0.5° latitude by 0.5° longitude) from the Estimating the Circulation and Climate of the Ocean simulation (ECCO2, Marshall et al., 1997) for the period January 1993 to December 2016 were used to obtain a more complete spatial pattern and temporary evolution of the BLT in the equatorial Pacific Ocean as well as in the salinity budget analysis. The data have a vertical resolution of ~10–15 m in the upper 150 m and 25–30 m from 150–300 m. As discussed in Guan et al. (2019), the ECCO2 product has been applied in many scientific studies and has been validated with observations of oceanic circulation and water properties (e.g., Ponte & Vinogradova, 2016).

Monthly near-surface current estimates from the Ocean Surface Current Analyses-Real time (OSCAR, Bonjean & Lagerloef, 2002) data set were also utilized. These data are available at 1/3° gridded resolution and we used data for the period January 1993 to December 2016.

Monthly surface winds are from the European Centre for Medium-Range Weather Forecasts (ECMWF, Dee & Uppala, 2009) from January 1979 to December 2016 with a gridded horizontal resolution of 0.75°. Sea Surface Height Anomaly (SSHA) is from the 1/4° gridded monthly Archiving, Validation, and Interpretation of Satellite Oceanography (AVISO, Ducet et al., 2000) data for the period October 1992 to December 2016. The monthly CMAP (Xie & Arkin, 1997) precipitation data on a 2.5° × 2.5° grid are available from January 1979 to December 2016. The evaporation (derived from the latent heat component) (available from January 1958 to December 2016) and net heat flux (available from January 1984 to December 2009), both on a 1° × 1° spatial grid, are from the Objective Analysis Flux (OAFlux; Yu & Weller, 2007).

The monthly anomaly for each of the data sets listed above is determined by removing the seasonal cycle at each grid point and, if needed, the data are then interpolated to a 1° × 1° grid. The "interannual" monthly time series is then obtained by filtering these monthly anomaly data with an 11-point symmetric filter (Trenberth, 1984). For the salinity budget analysis, the "noisy" advection terms are further filtered by a 3-point running mean in space.

The "moderate" and "extreme" El Niño events are defined by the same extreme events identified in Cai et al. (2014) and Zhong et al. (2019), which are based on the observed December to February rainfall during anomalously warm periods in the Niño3 region (150°W–90°W, 5°S–5°N). The extreme El Niño events are defined as the years that the rainfall in that region was greater than 5 mm per day. Seven El Niño events are present during the period of our study from January 1993 to December 2016 of which five events are classified as moderate (1994, 2002, 2004, 2006, and 2009), and two events are classified as extreme (1997, 2015) (Cai et al., 2014; Zhong et al., 2019). Composites of moderate and extreme El Niño events were obtained by averaging over all the events in each scenario. Composites for all fields constructed from the ECCO2 data include all the El Niño events in each scenario. Due to the limited TAO/TRITON data availability, only the 0°, 156°E site is used to construct the composites and these include only the extreme El Niño of 2015 and the moderate El Niños composited during 2002, 2004, and 2006 when data were available. Each individual El Niño event used to form the composite events from both the in situ mooring data and the ECCO2 product can be found in the Supplement (See Figures S1–S6). While some discrepancies exist between the individual events, for the most part they tend to support the major features of the temperature structure, the BLT and ILD structure, and their phasing with respect to the El Niño events as discussed for the composites in Section 3. Nonetheless, given the small sample size, the robustness of our results should be considered with caution. Since the net heat flux data is only available from January 1984 to December 2009, the extreme El Niño is only available during 1997 for the construction of the surface flux forcing.

In order to see the evolution of the BLT and forcing fields, the composited 24-month duration is shown beginning in January (0) during each of the El Niño events to December (+1) of the year following the El Niño event. The tropical Pacific maps of various fields are constructed to be the mean of the typical peak seasons, namely November (0) through January (+1) (referred to in the following as NDJ).

2.2. Methodology

The ILD is given by

$$\mathrm{ILD} = z\left(T = T_s - \Delta T\right) \tag{1}$$

where T_s is the temperature at 10 m and $\Delta T = 0.5°C$. Similarly, following Sprintall and Tomczak (1992), we estimate the MLD as:

$$\mathrm{MLD} = z\left(\rho\right) = \rho_s + \frac{\partial \rho}{\partial T}\Delta T \tag{2}$$

where ρ_s is the density at 10 m and $\Delta T = 0.5°C$. The BLT for each month (t) is then given by

$$\mathrm{BLT} = \mathrm{ILD} - \mathrm{MLD} \tag{3}$$

For cases when ILD < MLD, we assign BLT = 0. In our study, the ILD, MLD, and BLT are estimated using both the TAO/TRITON data at 0°, 156°E and 0°, 170°W and the complete ECCO2 output for the tropical Pacific.

3. Upper Ocean Stratification Characteristics

3.1. Mean State of the Equatorial Pacific Ocean

To have an overall picture of the equatorial Pacific Ocean mean state, we first show the standard deviation of the sea surface salinity anomaly and the mean BLT based on the ECCO2 output for the period January 1993 to December 2016 (Figure 1). The standard deviation shows that salinity variability is highest in the fresh warm pools of the western Pacific Ocean and in the far eastern tropical north Pacific. This is due to the high variability of precipitation in these regions. The maximum BLT in the mean is found in the equatorial western Pacific Ocean (about 30 m) and decreases eastward (about 10 m near 140°W). Note that this is the mean picture, which may reflect that the BL is only seasonally or sporadically present, such as in the eastern Pacific Ocean (e.g., Katsura & Sprintall, 2020), or alternatively that the ECCO vertical resolution is not sufficient to resolve the thin BLTs and shallow MLDs in this region.

The two stations that are the focus of our study represent the western Pacific Ocean warm pool region (0°, 156°E) and the central Pacific Ocean (0°, 170°W) (Figure 2). These two regions are also where significant changes from deep convection occur during moderate and extreme El Niños (see Figure 1 from Cai et al., 2014). Warm temperatures of >28°C characterize the surface layer at 0°N, 156°E. The thermocline depth is typically about 100 m, although shallower thermoclines are evident during the extreme El Niño events of 1997 and 2015 (Figure 2a). Over the time series, the salinity at 0°N, 156°E is typically fairly fresh (<34 psu) in the surface layer (Figure 2b). In contrast, the temperature at 0°N, 170°W is cooler, and frequently lower than 28°C while the surface layer is saltier, at around 35.5 psu (Figures 2c and 2d), compared to the western Pacific. However, as will be discussed further below, during El Niño events, the salinity in the central Pacific freshens relative to that in the western Pacific in response to the eastward shift in convection.

3.2. The BL at 0°N, 156°E and 0°N, 170°W

The composite of the MLD, ILD, and BLT during moderate and extreme El Niño events are estimated at 0°N, 156°E (Figure 3). During moderate events, the ILD is about 75 m during the developing phase and shoals to about 55 m during the mature phase and deepens again afterward. In contrast, the MLD is almost constant during the developing and mature phase (about 50 m) and shoals during the decaying phase (about 40 m). As a result, at 0°N, 156°E the BLT is nearly 20 m during the developing and decaying phases of moderate El Niños, but reduces to around 5 m during the peak season from November to January (Figure 3a). During extreme El Niño events, the BLT is about 20 m during the developing phase of El Niño but is near zero for the mature phase and afterward. This is mainly due to the shoaling of the ILD during the mature and decaying phase (Figures 3d and 3f).
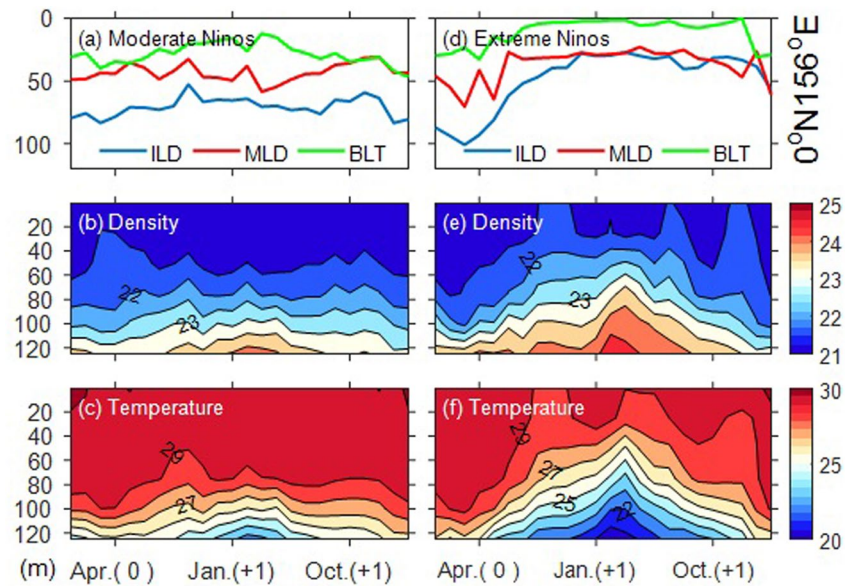
Figure 3. Composites of isothermal layer depth (ILD, blue line), mixed layer depth (MLD, red line) and BL Thickness (BLT, green line) computed from the TAO/TRITON mooring data at 0°, 156°E for the (a) moderate (1994, 2002, 2004, 2006) and (d) extreme El Niño events (1997 and 2015). Panels (b and e) are the same as (a and b) but for density. Panels (c and f) are the same as (a and b) but for temperature. The *x*-axis is 24 months, beginning in January(0) of the El Niño events to December(+1) of the year following the El Niño events. BL, barrier layer.

Since there are limitations in the complete time series of the in situ data from the TAO/TRITON array, we repeat the calculation with the ECCO2 product (Figure 4), which has no gaps in the data set and yet shows similar signals in the upper ocean stratification to those observed at the 0°, 156°E buoy. The ECCO2 product at 0°N, 156°E shows that during moderate El Niño events, the ILD is deeper during the developing and decaying phase of the El Niño, but shallower during the mature phase. This leads to a thicker BLT (about 40 m) before and after the mature phase of El Niño events (see Figures 4a, 4c and 4e). In contrast, during the extreme El Niño events the BLT is thick (about 40 m) during the developing phase and decreases to almost zero during the mature and decaying phase, this is mainly due to the shoaling ILD (Figures 4b, 4d and 4f). At 0°N, 156°E the depth of the 29°C isotherm is about 80 m before and after the mature phase of the moderate El Niño event, but shoals to about 60 m during the mature phase (Figure 4e). In contrast, during the extreme El Niño events, the depth of the 29°C isotherm is about 90 m during the developing phase and shoals to about 20 m during the mature phase before deepening again to about 90 m during the decay phase (Figure 4f).

Unlike at 0°N, 156°E, further east at 0°N, 170°W the BLT determined using the ECCO2 product is thicker (about 40 m) during the mature phase of moderate El Niño events but is non-existent before and afterward. This may indicate that during the mature phase of moderate El Niño events the deep convection related precipitation extends to at least 0°N, 170°W. During extreme El Niño events, the deepest ILD and MLD shift prior to the mature phase and last longer at 0°N, 170°W (see Figures 4g, 4h, 4j, and 4l) compared to 0°N, 156°E. The ILD also deepens from 45 to 85 m after the mature phase of extreme El Niño events at 0°N, 170°W (Figures 4h and 4l). During extreme El Niño events the temperature decreases from 30°C during the developing and mature phase and drops to about 24°C afterward (Figure 4l). During moderate El Niños, the surface temperature is about 28°C before and after the mature phase, but reaches 30°C during the mature phase (Figure 4k). This is consistent with the extension of the western Pacific Warm pool region.

3.3. Spatial Distribution of the Upper Ocean Characteristics

Spatial distribution of the BLT, ILD, and MLD in the Pacific Ocean determined using ECCO2 are shown composited during the peak season (November(0)–January(+1)) for moderate (Figures 5a, 5d and 5g) and
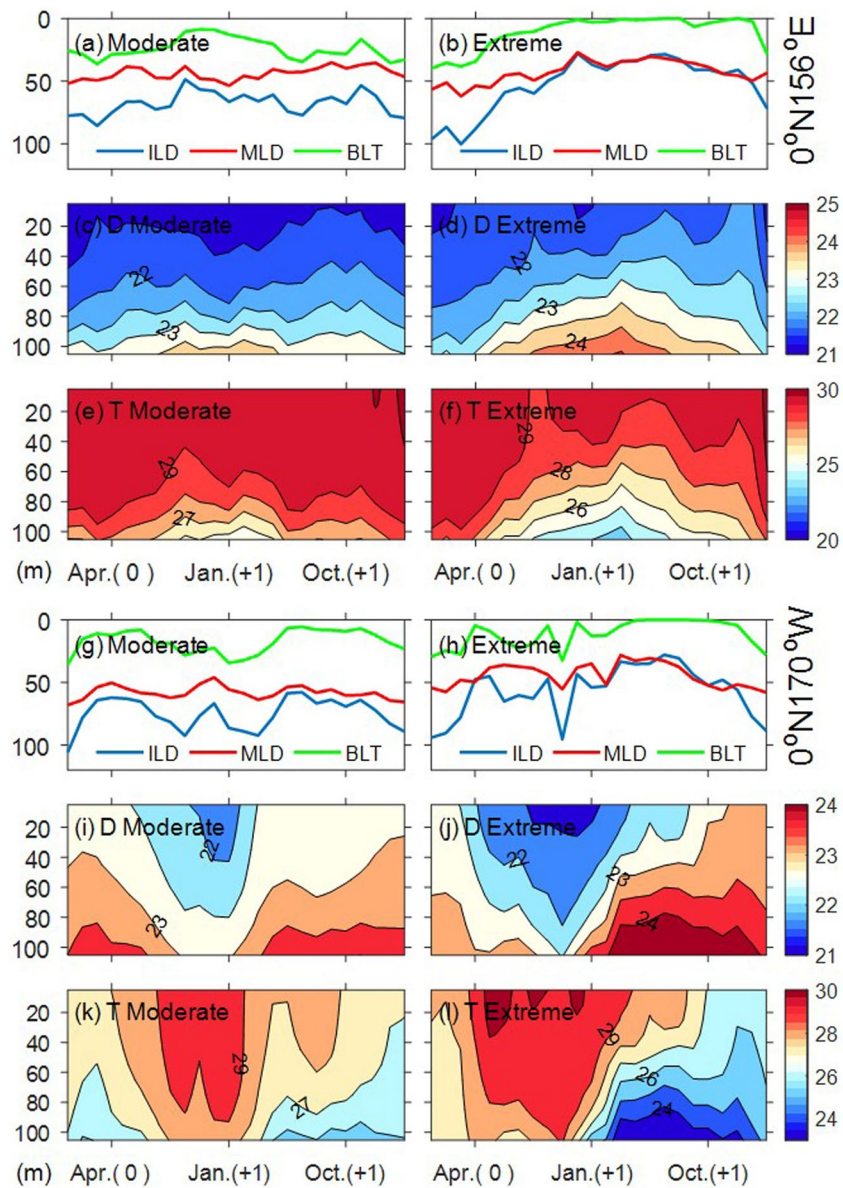
Figure 4. Composite of ILD (blue line), MLD (red line), and BLT (green line) for the (a) moderate and (b) extreme El Niño events at 0°, 156°E based on ECCO2. Composite of density and temperature for the (c, e) moderate and (d, f) extreme El Niño years, respectively. Panels (g–l) are the same as (a–f), but at 0°, 170°W based on ECCO2. The *x*-axis is 24 months, beginning in January(0) of the El Niño event to December(+1) of the year following the El Niño event. ILD, isothermal layer depth; ECCO2, Estimating the Circulation and Climate of the Ocean; MLD, mixed layer depth.

extreme El Niño events (Figures 5b, 5e and 5h) and their differences (Figures 5c, 5f and 5i). Here the difference is calculated by subtracting the composite of extreme El Niños from the moderate El Niños.

During moderate El Niños, the BLT is thickest (about 30 m) in the central-western Pacific Ocean (150°E to 130°W) between 10°S and 10°N (Figure 5a). During extreme El Niños, the BL is thinner (about 20 m) and is located further eastward and largely confined to the equatorial region (Figure 5b). Thus, the BL is thicker (~15 m) in the western Pacific Ocean and shallower (~10 m) in the eastern Pacific Ocean (Figure 5c) in moderate events compared to extreme events. In general, the composite of ILD and MLD during the moderate and extreme El Niños (Figures 5d–5i) supports the patterns found in Figure 4. The ILD and MLD are deeper during moderate El Niños (Figures 5f and 5i), and the deeper ILD, particularly in the western Pacific, results in a thicker BL.
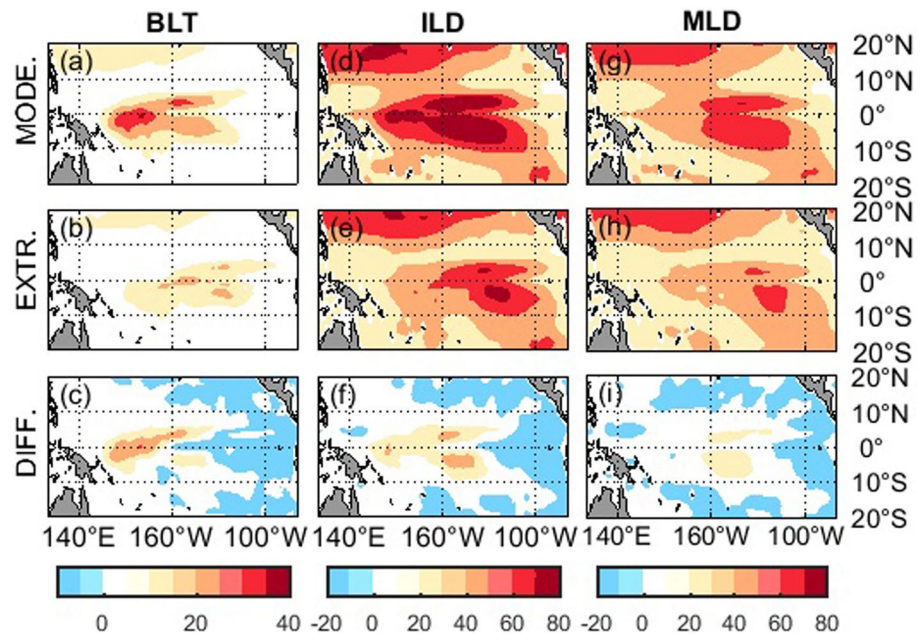
Figure 5. The BL thickness (left), isothermal layer depth (middle) and mixed layer depth (right) for composite moderate El Niños (a,d,g) and extreme El Niño (b, e, h) events and their differences (c, f, i) based on ECCO2. The difference is calculated by subtracting the composite of extreme El Niños from moderate El Niños. BL, barrier layer; ECCO2, Estimating the Circulation and Climate of the Ocean.

Figure 6 shows the composites of ILD, MLD, and BLT along the equator for the moderate and extreme El Niños based on the ECCO2 output. During extreme El Niños, the thickest BLTs along the equator extend further eastward to ~120°W compared to moderate events (Figures 6c and 6f). Initially from January(0)
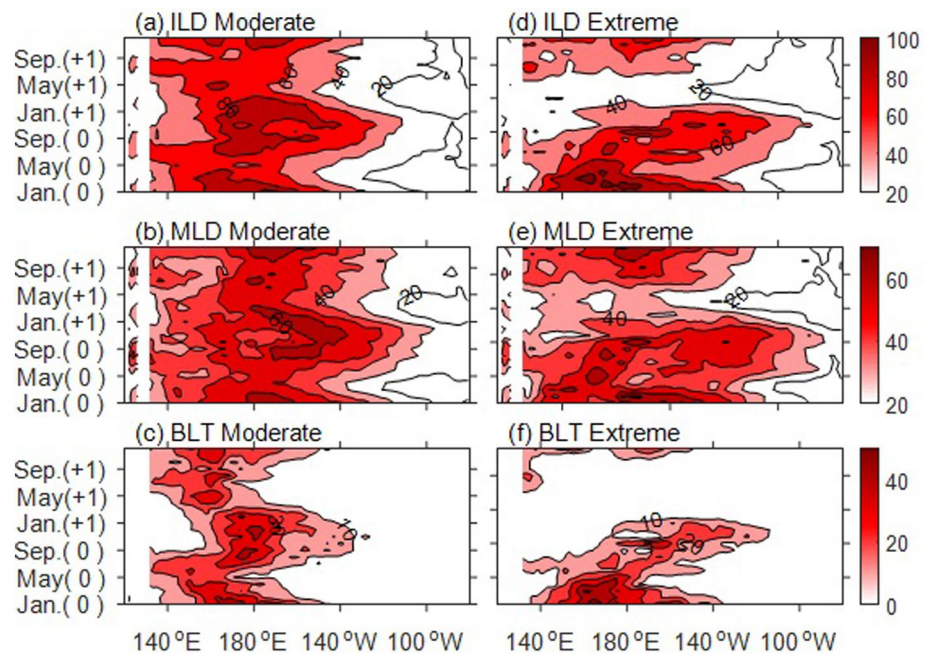

Figure 6. Composite of ILD (top), MLD (middle) and BLT (lower) along the equator in the Pacific Ocean for the moderate (a–c) and extreme (d–f) El Niños based on ECCO2. The y-axis is 24 months, beginning in January (0) of the El Niño event to December (+1) of the year following an El Niño event. ILD, isothermal layer depth; ECCO2, Estimating the Circulation and Climate of the Ocean; MLD, mixed layer depth.
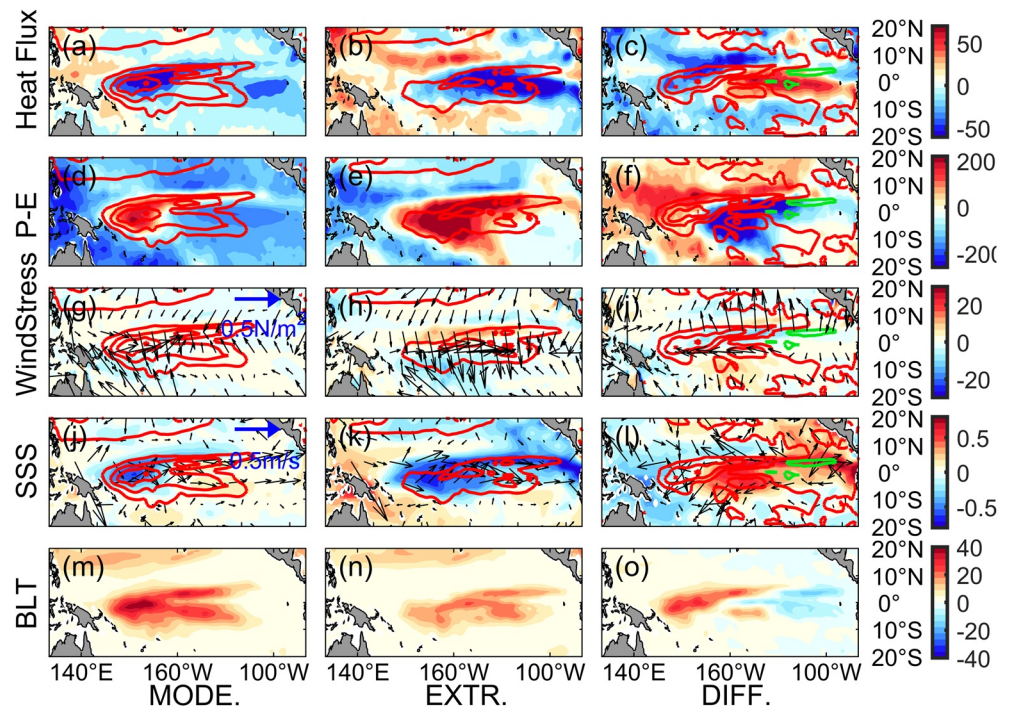
Figure 7. Composite of monthly anomalous net heat flux (W m^{-2}) (a–c); precipitation minus evaporation (cm yr^{-1}) (d–f), wind stress (N/m^2, vectors) and its curl (N/m^{3}x10^8, colors) (g–i); ocean current (m/s, vectors), SSS (colors) (j–l); and Barrier Layer Thickness (m–o) during the mature phases (NDJ averaged) of moderate El Niños (a, d, g, j, m), extreme El Niños (b, e, h, k, n), and their difference (c, f, i, l, o). The difference is estimated by subtracting average of extreme El Niños from the moderate El Niños. The overlain red (green) contours are the positive (negative) BLT, and given at 10 m intervals.

to May(0), the BLT during extreme events is >40 m but then they quickly thin extending further eastward before largely disappearing following the peak El Niño period (January(+1)). In contrast, the BLTs during the moderate El Niños are ~30 m thick and west of ~160°W remain throughout the evolution of the event (Figure 6c). In the western Pacific Ocean, the differences in BLT between the peak phase of moderate and extreme El Niño events are mainly due to the deeper ILD and MLD (Figures 6a–6f), especially the deeper ILD. Namely during the moderate El Niño events, the ILD is deeper (about 80 m) during the mature phase compared to an ILD of ~40 m during the extreme El Niños. In the western equatorial Pacific Ocean, the MLD during moderate events is about 50 m compared to 30 m during the extreme events.

To summarize, our analysis suggests that overall the BLT is thicker initially during extreme El Niño but then quickly erodes, whereas during moderate El Niños the BLT is relatively thick but lasts longer and is more confined to the western Pacific. In the western equatorial Pacific Ocean, during the mature phase the BLT is thicker during moderate El Niños compared to extreme El Niños, which is mainly due to a deeper ILD compared to the MLD. In the following, we will explore the possible mechanisms responsible for the thickening of the BLT during the mature phase of moderate events in the western equatorial Pacific Ocean.

4. The Atmospheric and Oceanic Conditions during the Moderate and Extreme El Niños

To explore the possible mechanisms responsible for the BL differences during moderate and extreme El Niños, the anomalous atmospheric and oceanic conditions that exist during the two types of events are examined. The composite of the monthly anomalous net heat flux, net freshwater flux (precipitation minus evaporation), wind stress (vectors) and its curl (contours) and the ocean surface current during the mature phase (NDJ averaged) of moderate El Niños (Figures 7a, 7d, 7g, and 7j), extreme El Niños (Figures 7b, 7e, 7h, and 7k), and their difference (Figures 7c, 7f, 7i and 7l) are computed for the events during the period

of January 1993 to December 2016. Here the difference is estimated by subtracting the average of extreme El Niños from the moderate El Niños. We have shown above that during the mature phase (i.e., November(0) through January(+1)) of the moderate El Niños, the BL is thicker in the equatorial western Pacific Ocean, which is mainly due to a deeper ILD (Figure 5). The location of the thickest BLTs coincides with the maximum anomalous net heat flux and also with where the anomalous P-E > 0 (i.e., where there is a net freshwater flux into the ocean compared to the mean) (Figure 7). More specifically, during both extreme and moderate El Niños, the BLT coincides with the anomalous net heat flux and the anomalous net heat flux is less negative for the moderate El Niños, which means that less heat is removed from the ocean and leads to a deeper ILD. In terms of freshwater flux, during extreme El Niños the P-E is anomalously more positive, which means that there is more freshwater input into the ocean (compared to the mean) that acts to further shoal the MLD. The anomalous zonal eastward current is stronger during extreme El Niños (Figure 7k) and so potentially advects the thicker mean BL from west to east (see Figure 1). The wind stress curl is also anomalously stronger during extreme El Niños and the anomalous Ekman pumping is therefore also stronger, and so results in a shallower ILD and thinner BLT.

5. Salinity Budget Analysis

A mixed layer salinity budget is constructed using the ECCO2 output to diagnose the processes that might be responsible for the shallow haline stratification along the equator in the Pacific during the moderate and extreme El Niño events. Following Ren et al. (2011), the salinity budget analysis equation is expressed as:

$$\frac{\partial S_m}{\partial t} = \frac{(E - P) S_m}{h_m} - v \cdot \nabla S_m - \frac{w_e \Delta S}{h_m} + \varepsilon \tag{4}$$

with

$$w_e = w_{EK} + w_m = \frac{\nabla \times \tau}{\rho f} + \left(\frac{\partial h_m}{\partial t} + \nabla \cdot h_m \, \overline{v} \right) \tag{5}$$

Here, τ denotes wind stress, $\rho = 1{,}026$ kg/m^3 is the seawater density, f is Coriolis frequency, h_m is MLD, S_m is mixed layer salinity, ΔS is the salinity difference between S_m, and the salinity at the depth 20 m below the MLD, E is evaporation, P is precipitation, and ε is the residual term. The entrainment velocity w_e is given in Equation 5 which is comprised of the Ekman velocity (w_{EK}) and the mixing velocity (w_m). The Ekman velocity w_{EK} corresponds to the upwelling (downwelling) generated by the convergence (divergence) of the horizontal wind-driven Ekman transport as defined by the first term on the right hand side of Equation 5 (Yu, 2011). The mixing velocity w_m can be separated into local tendency of the MLD ($(\partial h_m)/\partial t$) and the horizontal advection term $\nabla \cdot h_m \, v$, where v is the surface current (including both the Ekman and geostrophic currents).

During both moderate and extreme El Niños, the surface freshwater flux (E-P) term dominates along the equator (Figures 8c and 8d). During the extreme El Niño events, there is more precipitation in the central Pacific Ocean and across the equatorial Pacific Ocean such that the net freshwater flux extends further eastward and is closer to the equator. This is also what we expect based on Cai et al. (2014). Moreover, the tendency of mixed layer salinity changes is positive in the northern hemisphere and negative in the southern hemisphere, which corresponds to an increasing mixed layer salinity in the northern hemisphere and decreasing mixed layer salinity in the southern hemisphere (Figure 8b). In contrast, during the peak phase of moderate El Niños mixed layer salinity increases in the western Pacific Ocean but becomes fresher in the far western Pacific Ocean. In the far western Pacific during both moderate and extreme events, the advection term ($-\overline{v} \cdot \nabla S_m$) dominates north of the equator (Figures 8e and 8f; positive means that lower salinity is advected westward) and surface freshwater flux acts to dampen this impact (Figures 8a and 8b). The entrainment term tends to increase the mixed layer salinity in the northern hemisphere and in the southwestern Pacific Ocean during moderate El Niño events. During extreme El Niño events, the increased salinity due to entrainment is even stronger in the northern and southwestern Pacific Ocean, although entrainment acts to decrease the mixed layer salinity in the northwestern Pacific Ocean (Figures 8g and 8h). The entrainment term is mainly dominated by the mixing velocity term w_m near the equator, which varies mainly in response
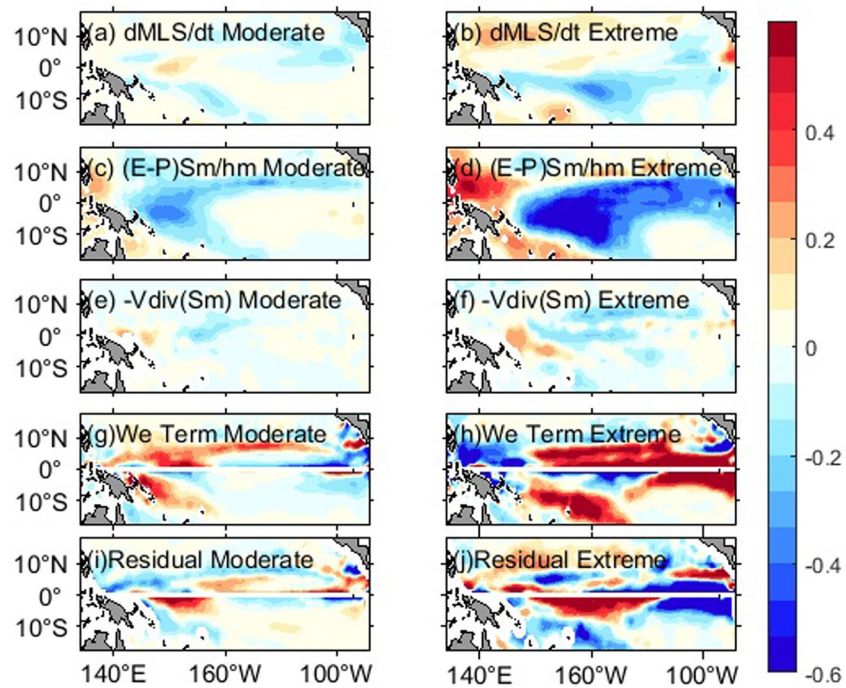
Figure 8. Composite of the terms in the salinity budget constructed from the ECCO2 product including the (a, b) mixed layer salinity (MLS) tendency, (c, d) tendency caused by surface freshwater flux term, (e, f) divergence term, (g, h) entrainment term and (i, j) residual during the mature phase of the moderate (a, c, e, g, i) and extreme (b, d, f, h, j) El Niños. The units for all terms are $\times 10^{-7}$ $psus^{-1}$. ECCO2, Estimating the Circulation and Climate of the Ocean.

to the meridional advection term (Equation 5). The residual term, calculated as the left hand side minus the sum of right hand side of Equation 4 (see Figures 8i and 8j), is largest near the equator, which may be due to the neglection of the nonlinear terms or reflect the large uncertainty in the entrainment term.

We further separate the advection terms into the zonal and meridional advection components (Figure 9). A positive (negative) divergence term ($-v \cdot \nabla S_m > 0$) means that mixed layer salinity increases (decreases). Near the equator, in general the meridional advection dominates while away from the equator the zonal advection terms play a more important role. Near the equatorial central Pacific (180°E−155°W), the divergence term is negative (i.e., $-v \cdot \nabla S_m < 0$) (Figures 9a and 9b) and the meridional advection term (Figures 9e and 9f) becomes important. The negative divergence term implies that the mixed layer salinity in the central equatorial Pacific decreases due to the divergence. In contrast, in the Western Pacific Ocean, the divergence term is positive (i.e., $-v \cdot \nabla S_m > 0$) (Figures 9a and 9b), so the mixed layer salinity increases due to the divergence of salinity and is dominated by the zonal advection terms (Figures 9c and 9d). The typical deep convection in the western Pacific Ocean lowers the mean salinity compared to the east (i.e., there is a fresh pool in the western Pacific Ocean in the mean state) therefore the salinity increases zonally ($\partial S/\partial x > 0$) and meridionally ($\partial S/\partial y > 0$) especially during the moderate El Niño events (see Figure 7j, color shading), which suggests that v' < 0 (i.e., a southward meridional current anomaly) and u' < 0 (a westward zonal current anomaly).

In summary, the analysis of the mixed layer salinity budget reveals a dominant role of the surface freshwater flux in the generation of salinity anomalies within the equatorial Pacific Ocean. In the central Pacific, the mixed layer salinity decreases and both meridional and zonal advection are responsible for the freshening. In the far western Pacific during both moderate and extreme events, the salinity advection term is westward and dominates north of the equator but the surface freshwater flux acts to dampen this impact.
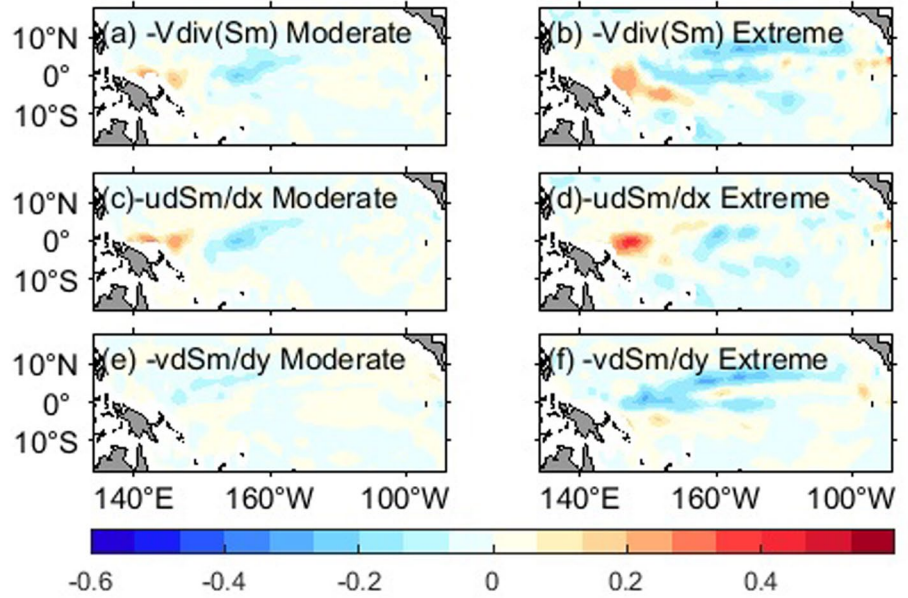
Figure 9. The divergence term ($-\vec{v} \cdot \nabla S_m$) in the salinity budget (a, b), induced by (c, d) zonal advection ($-u\partial S_m / \partial x$) and (e, f) meridional advection ($-v\partial S_m / \partial y$) during the moderate (a, c, e) and extreme (b, d, f) El Niño events. The units for all terms are $\times 10^{-7}$ $psu s^{-1}$.

6. Impact of the BL on the Upper Layer Circulation

Zonal movement of the western equatorial fresh/warm pool of water is fundamental to ENSO dynamics (Bosc et al., 2009; Cronin & McPhaden, 1998; Delcroix & Picaut, 1998; Picaut et al. 1996, 2001; Qu et al., 2014). Monthly salinity anomalies as large as 1 psu are common in the western equatorial Pacific as the warm, fresh pool and the BL at its eastern edge move eastward during El Niño over distances of thousands of kilometers. As shown in the previous section, the anomalous zonal eastward current is stronger during extreme El Niños, advecting the thicker BLs from west to east. The total zonal current during El Niños is dominated by a "freshwater jet" in the western Pacific Ocean in response to the presence of BLs (Roemmich et al., 1994; Zhang & Clarke, 2015). In this section, we examine the role of this jet on the dynamics occurring during the two different El Niño strengths.

Following Zhang and Clarke (2015), the fresh-water flux impact on the zonal geostrophic current at 1°S, 156°E, 0°N, 156°E, and 1°N, 156°E is calculated using the TAO/TRITON time series of T and S (Figure 10). The contribution to the current from the monthly anomalous salinity (u_F) and temperature (u_T) effect off the equator is given by

$$u_F = f^{-1}g\left[\int_{-ILD}^{0} \beta_S S' dz\right]_y \tag{6}$$

$$u_T = -f^{-1}g\left[\int_{-ILD}^{0} \alpha_T T' dz\right]_y \tag{7}$$

and on the equator (where $f = 0$) by:

$$u_F = \beta^{-1}g\left[\int_{-ILD}^{0} \beta_S S' dz\right]_{yy} \tag{8}$$
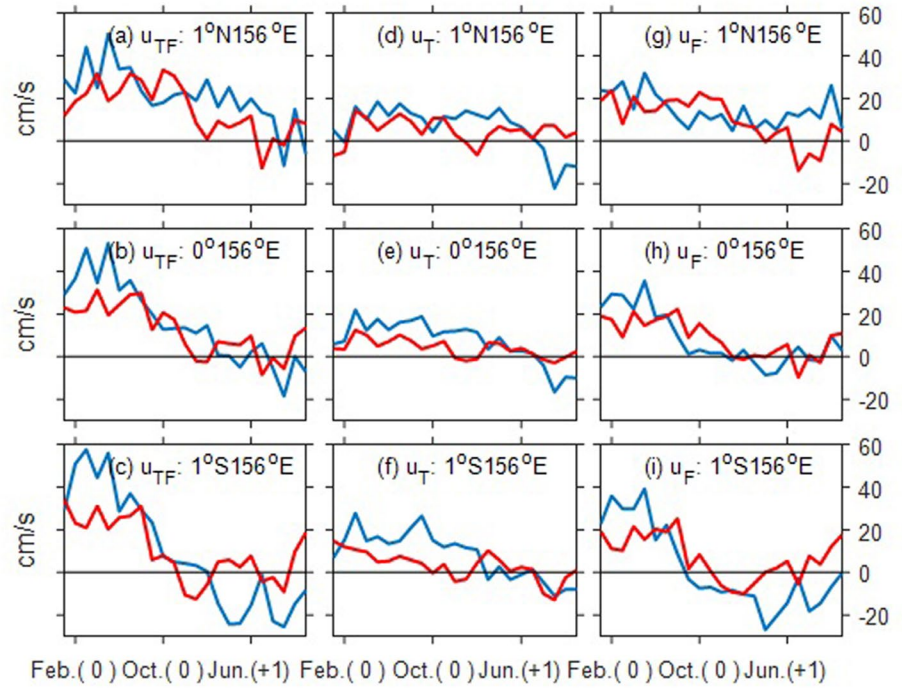
Figure 10. The freshwater flux induced current at 1°N, 156°E (a), 0°N, 156°E (b) and 1°S, 156°E (c) for moderate El Niños (red lines) and extreme El Niños (blue lines). Panels (d–f) are the same as (a–c), but for the temperature contribution to the total zonal current and panels (g–i) for the salinity contribution to the total zonal current. The *x*-axis is 24 months, beginning in January(0) of the El Niño events to December(+1) of the year following El Niño events. u_{TF} is the zonal current related to the freshwater flux, u_T is the temperature contribution, and u_F is the salinity contribution. The units are cm/s.

$$u_T = -\beta^{-1}g\left[\int_{-\mathrm{ILD}}^{0} \alpha_T T' dz\right]_{yy} \tag{9}$$

In Equations 6–9, f is the Coriolis parameter, $\beta = df/dy$ off the equator, $g = 9.8$ m/s² is the gravitational acceleration, $\beta_S = 7.5 \times 10^{-4}$ is the salinity contraction coefficient and $\alpha_T = 3.3 \times 10^{-4}$ °C⁻¹ is the thermal expansion coefficient, S′ is the monthly salinity anomaly, and T′ is the monthly temperature anomaly. The salinity (temperature) induced dynamic height is estimated by integrating the monthly salinity (temperature) anomaly over the ILD. The total zonal current, u_{TF}, is given by the summation of Equations 6 and 7 off the equator and Equations 8 and 9 on the equator. Thus, u_{TF} represents the current that includes both the thermosetric and halosteric contribution. Physically, this means that if there is a negative salinity anomaly (S' < 0), corresponding to a freshening anomaly, the water in the isothermal layer is less dense and so to keep the pressure at the isothermal layer depth constant, the sea level must slightly increase. Based on the idea that the zonal scale is much larger than the meridional scale, to a first approximation the low-frequency zonal flow is geostrophically balanced (see Zhang & Clarke, 2015 for a detailed discussion). The associated low-frequency zonal geostrophic current at 1°N, 156°E is thus estimated based on the in situ temperature and salinity data at 2°N, 156°E and 0°N, 156°E. Whereas on the equator (0°N, 156°E), u_{TF} (u_F, u_T) are estimated based on the temperature and salinity at the three stations (2°S, 156°E, 0°N, 156°E, and 2°N, 156°E).

In Figure 10, we show the salinity and temperature induced zonal current anomaly during extreme (blue line) and moderate (red line) El Niños. Since under the mean state, the zonal current in the western Pacific Ocean is westward, here when there is a positive (negative) total zonal current anomaly (u_{TF}), it means a weakening (strengthening) of the westward zonal current. Thus, during the extreme El Niños (blue line in Figure 10), the eastward current anomaly is stronger (about 60 cm/s) during the developing phase (January(0)–September(0)) of the events compared to the total current anomaly (about 30 cm/s) during mod-

erate El Niño events (red line in Figure 10) especially at 1°S, 156°E (Figures 10a–10c). This eastward zonal current anomaly pushes the warm pool edge eastward. During the decaying phase of El Niño events (June(+1)–December(+1)), the eastward current anomaly becomes almost zero (Figures 10a–10c). During the extreme El Niño events, there is a shift to a westward current anomaly. This suggests that the negative feedback following extreme El Niños is stronger than during the moderate scenarios.

Furthermore, the salinity and temperature induced zonal current anomaly based on Equations 6–9 shows that salinity anomalies (i.e., the halosteric contribution) are the main causes for this change in the total current anomalies (i.e., u_F is about 30 cm/s while u_T is about 20 cm/s) at all three stations (1°S, 156°E; 0°N, 156°E; and 1°N, 156°E).

7. Summary and Discussion

In this paper, the BL in the equatorial Pacific Ocean during moderate and extreme El Niños was studied using TAO/TRITON data and ECCO2 output. Our analysis shows that in the western Pacific Ocean, the ILD deepens during moderate El Niño events and then shoals during the year following the event. This phenomenon is even more obvious during extreme El Niños. The ILD deepens during the developing phase but shoals during the peak phase of the El Niño events.

Using in situ data and ECCO2 output, the composite of BLT, MLD, and ILD during extreme and moderate El Niños shows that during the peak months of El Niño events (November(0) to January(+1)), the BLT is thicker in the western Pacific Ocean during moderate El Niños compared to extreme El Niños, which is mainly due to a deeper ILD compared to the MLD. Moreover, at 0°N, 156°E before the peak months of the El Niño event, the BL thickens during extreme El Niño years compared to moderate El Niño years. This is mainly due to the deepening ILD. Maes et al. (2002) pointed out that the presence of the BL is important for the development of El Niño as removing the BL reduces the build-up of the heat in the western Pacific Ocean. This perhaps explains why we see thicker BLT before extreme El Niños, and furthermore that they may be responsible for the increased heat buildup that leads to the extreme El Niño events.

A salinity budget analysis shows that the freshwater flux and advection are the main reasons for the BLT differences during the two types of El Niño events. Furthermore, the result of the mixed layer salinity budget reveals a dominant role of the surface freshwater flux in the generation of salinity anomalies along the equatorial Pacific Ocean. But in the far western Pacific Ocean and central Pacific Ocean, the divergence term also contributes. The whole process can be summarized in the schematic (see Figure 11). Namely, during moderate El Niños, the anomalous net heat flux is less negative, which means that less heat is removed from the ocean and this leads to a deeper ILD. In terms of freshwater flux, during extreme El Niños the P-E is anomalously more positive, which means that there is more freshwater input into the ocean (compared to the mean) that acts to further shoal the MLD. The anomalous zonal eastward current is stronger during extreme El Niños (Figure 7k) and so potentially advects the thicker BLT from west to east (see Figure 1). The wind stress curl is also anomalously stronger during extreme El Niños and the anomalous Ekman pumping is therefore also stronger, and so this acts to shoal the ILD and produces a thinner BLT.

Lastly, our study shows that during both moderate and extreme El Niños, the zonal current anomaly related to the freshwater flux is not negligible (about 18 cm/s). In addition, during extreme El Niños, the fresh zonal current anomaly is stronger before and after the event, especially at 1°S, 156°E. The current is mainly driven by the salinity effect. The existence of near-surface relatively fresh equatorial flow was first documented by Roemmich et al. (1994) who observed an extremely fresh salinity anomaly within an equatorial jet over several months occurring in a surface layer 50 m thick. Beneath this fresh layer was a sharp halocline that occurred in an isothermal layer, in other words, a BL existed. However, the Roemmich et al. (1994) theory is only appropriate over short periods of about 10 days. On longer time scales, our study suggests that during the development of extreme El Niños, the presence of a thicker BLT helps in the build-up of heat that is transported east in the freshwater jet, which further leads to the occurrence of the extreme El Niño events.

Brown et al. (2014) have shown that many of the state-of-the-art Coupled Model Intercomparison Project Phase 5 (CMIP5) models poorly represent the salinity variability at the warm pool edge and so would seem to be missing a basic component of the coupling dynamics. Furthermore, since the zonal movement of the
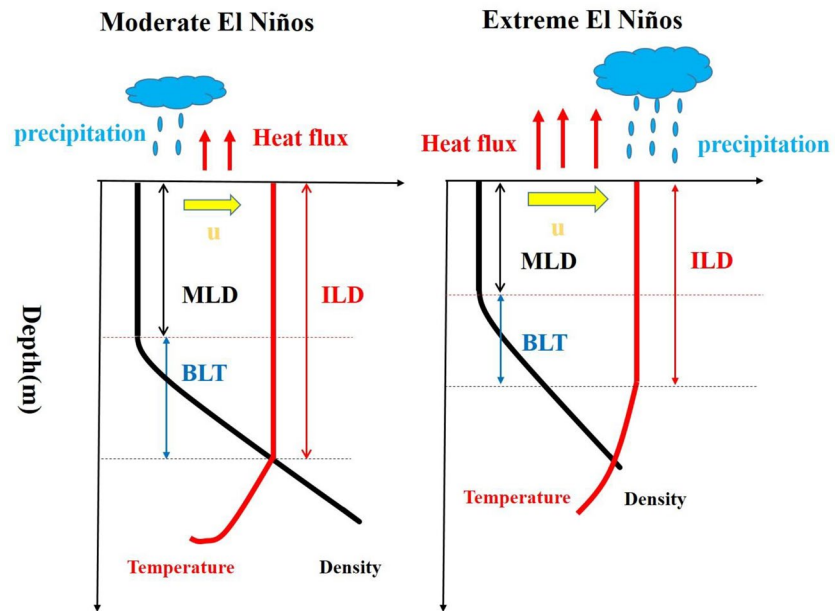
Figure 11. Schematic of the mixed layer characteristics during (left) moderate and (right) extreme El Niños. MLD is the mixed layer depth, ILD is Isothermal Layer Depth, and BLT is BL Thickness. BL, barrier layer; ILD, isothermal layer depth; MLD, mixed layer depth.

western equatorial fresh/warm pool of water is fundamental to ENSO dynamics (Bosc et al., 2009; Cronin & McPhaden, 1998; Delcroix & Picaut, 1998; Picaut et al. 1996, 2001; Qu et al., 2014), our study also provides further information about the strength, spatial structure of the interannual flow related to this zonal movement. This helps to improve our understanding of the ENSO dynamics during the two different El Niño regimes.

Data Availability Statement

Data sets used in this study can be found at the following websites: TAO/TRITON: https://www.pmel.noaa.gov/tao/drupal/disdel/; ECCO2: http://www.ecco-group.org/; Oscar Currents: https://podaac.jpl.nasa.gov/dataset/OSCAR_L4_OC_third-deg/; AVISO SSHA: https://www.aviso.altimetry.fr/en/data.html. Precipitation: http://www.esrl.noaa.gov/psd/data/gridded/data.cmap.html. Evaporation (derived from the latent heat component) and the net heat flux are from OAFlux: http://oaflux.whoi.edu/data.html. ECMWF Windstress data: http://apps.ecmwf.int/datasets/.

References

Bonjean, F., & Lagerloef, G. S. E. (2002). Diagnostic model and analysis of the surface currents in the tropical Pacific Ocean. *Journal of Physical Oceanography*, *32*, 2938–2954. https://doi.org/10.1175/1520-0485(2002)032<2938:dmaaot>2.0.co;2

Bosc, C., Delcroix, T., & Maes, C. (2009). Barrier layer variability in the western Pacific warm pool from 2000 to 2007. *Journal of Geophysical Research*, *114*, C06023. https://doi.org/10.1029/2008jc005187

Brown, J. N., Langlais, C., & Maes, C. (2014). Zonal structure and variability of the western Pacific dynamic warm pool edge in CMIP5. *Climate Dynamics*, *42*, 3061–3076. https://doi.org/10.1007/s00382-013-1931-5

Cai, W., Borlace, S., Lengaigne, M., van Rensch, P., Collins, M., Vecchi, G., et al. (2014). Increasing frequency of extreme El Niño events due to greenhouse warming. *Nature Climate Change*, *4*, 111–116. https://doi.org/10.1038/nclimate2100

Cronin, M. F., & McPhaden, M. J. (1998). Upper ocean salinity balance in the western equatorial Pacific. *Journal of Geophysical Research*, *103*, 27567–27587. https://doi.org/10.1029/98JC02605

Cronin, M. F., & McPhaden, M. J. (2002). Barrier layer formation during westerly wind bursts. *Journal of Geophysical Research*, *107*, SRF211–SRF2112. https://doi.org/10.1029/2001JC001171

Dee, D. P., & Uppala, S. (2009). Variational bias correction of satellite radiance data in the ERA-Interim reanalysis. *Quarterly Journal of the Royal Meteorological Society*, *135*, 1830–1841. https://doi.org/10.1002/qj.493

Delcroix, T., & Picaut, J. (1998). Zonal displacement of the western equatorial Pacific "fresh pool". *Journal of Geophysical Research*, *103*, 1087–1098. https://doi.org/10.1029/97JC01912

Ducet, N., Le Traon, P. Y., & Reverdin, G. (2000). Global high-resolution mapping of ocean circulation from TOPEX/Poseidon and ERS-1 and -2. *Journal of Geophysical Research*, *105*, 19477–19498. https://doi.org/10.1029/2000jc900063

Foltz, G. R., & McPhaden, M. J. (2009). Impact of Barrier Layer Thickness on SST in the Central Tropical North Atlantic*. *Journal of Climate*, *22*(2), 285–299. https://doi.org/10.1175/2008jcli2308.1

Girishkumar, M. S., Ravichandran, M., McPhaden, M. J., & Rao, R. R. (2011). Intraseasonal variability in barrier layer thickness in the south central Bay of Bengal. *Journal of Geophysical Research*, *116*(C3), C03009. https://doi.org/10.1029/2010jc006657

Godfrey, J. S., & Lindstrom, E. J. (1989). The heat budget of the equatorial western Pacific surface mixed layer. *Journal of Geophysical Research*, *94*(C6), 8007–8017. https://doi.org/10.1029/jc094ic06p08007

Guan, C., Hu, S., McPhaden, M. J., Wang, F., Gao, S., & Hou, Y. (2019). Dipole structure of mixed layer salinity in response to El Niño-La Niña asymmetry in the Tropical Pacific. *Geophysical Research Letters*, *46*(21), 12165–12172. https://doi.org/10.1029/2019gl084817

Katsura, S., & Sprintall, J. (2020). Seasonality and Formation of Barrier Layers and Associated Temperature Inversions in the Eastern Tropical North Pacific. *Journal of Physical Oceanography*, *50*(3), 791–808. Retrieved from https://journals.ametsoc.org/view/journals/phoc/50/3/jpo-d-19-0194.1.xml

Lukas, R., & Lindstrom, E. (1991). The mixed layer of the western equatorial Pacific Ocean. *Journal of Geophysical Research*, *96*, 3343–3357. https://doi.org/10.1029/90jc01951

Maes, C., Picaut, J., & Belamari, S. (2002). Salinity barrier layer and onset of El Niño in a Pacific coupled model. *Geophysical Research Letters*, *29*(24), 591–594. https://doi.org/10.1029/2002GL016029

Maes, C., Picaut, J., & Belamari, S. (2005). Importance of the salinity barrier layer for the buildup of El Niño. *Journal of Climate*, *18*, 104–118. https://doi.org/10.1175/jcli-3214.1

Marshall, J., Adcroft, A., Hill, C., Perelman, L., & Heisey, C. (1997). A finite-volume, incompressible Navier Stokes model for studies of the ocean on parallel computers. *Journal of Geophysical Research*, *102*(C3), 5753–5766. https://doi.org/10.1029/96jc02775

Mignot, J., de Boyer Montégut, C., & Tomczak, M. (2009). On the porosity of barrier layers. *Ocean Science*, *5*(3), 379–387. https://doi.org/10.5194/os-5-379-2009

Parampil, S. R., Gera, A., Ravichandran, M., & Sengupta, D. (2010). Intraseasonal response of mixed layer temperature and salinity in the Bay of Bengal to heat and freshwater flux. *Journal of Geophysical Research*, *115*(C5). https://doi.org/10.1029/2009jc005790

Picaut, J., Ioualalen, M., Delcroix, T., Masia, F., Murtugudde, R., & Vialard, J. (2001). The oceanic zone of convergence on the eastern edge of the Pacific warm pool: A synthesis of results and implications for El Niño-Southern Oscillation and biogeochemical phenomena. *Journal of Geophysical Research*, *106*, 2363–2386. https://doi.org/10.1029/2000JC900141

Picaut, J., Ioualalen, M., Menkes, C., Delcroix, T., & McPhaden, M. J. (1996). Mechanism of the zonal displacements of the Pacific warm pool: Implications for ENSO. *Science*, *274*, 1486–1489. https://doi.org/10.1126/science.274.5292.1486

Ponte, R. M., & Vinogradova, N. T. (2016). An assessment of basic processes controlling mean surface salinity over the global ocean. *Geophysical Research Letters*, *43*(13), 7052–7058. https://doi.org/10.1002/2016GL069857

Qu, T., Song, Y. T., & Maes, C. (2014). Sea surface salinity and barrier layer variability in the equatorial Pacific as seen from Aquarius and Argo. *Journal of Geophysical Research: Oceans*, *119*, 15–29. https://doi.org/10.1002/2013JC009375

Ren, L., Speer, K., & Chassignet, E. P. (2011). The mixed layer salinity budget and sea ice in the Southern Ocean. *Journal of Geophysical Research*, *116*(C8). https://doi.org/10.1029/2010jc006634

Roemmich, D., Morris, M., Young, W. R., & Donguy, J. R. (1994). Fresh equatorial jets. *Journal of Physical Oceanography*, *24*(3), 540–558. Retrieved from https://journals.ametsoc.org/view/journals/phoc/24/3/1520-0485_1994_024_0540_fej_2_0_co_2.xml

Sprintall, J., & Tomczak, M. (1992). Evidence of the barrier layer in the surface layer of the tropics. *Journal of Geophysical Research*, *97*, 7305–7316. https://doi.org/10.1029/92jc00407

Thadathil, P., Muraleedharan, P. M., Rao, R. R., Somayajulu, Y. K., Reddy, G. V., & Revichandran, C. (2007). Observed seasonal variability of barrier layer in the Bay of Bengal. *Journal of Geophysical Research: Oceans*, *112*(C2). https://doi.org/10.1029/2006jc003651

Thadathil, P., Thoppil, P., Rao, R. R., Muraleedharan, P. M., Somayajulu, Y. K., Gopalakrishna, V. V., et al. (2008). Seasonal variability of the observed barrier layer in the Arabian Sea*. *Journal of Physical Oceanography*, *38*(3), 624–638. https://doi.org/10.1175/2007/JPO3798.110.1175/2007jpo3798.1

Trenberth, K. E. (1984). Signal versus noise in the Southern Oscillation. *Monthly Weather Review*, *112*, 326–332. https://doi.org/10.1175/1520-0493(1984)112<0326:svnits>2.0.co;2

Vialard, J., & Delecluse, P. (1998). An OGCM study for the TOGA decade. Part I: Role of salinity in the physics of the western Pacific fresh pool. *Journal of Physical Oceanography*, *28*, 1071–1088. https://doi.org/10.1175/1520-0485(1998)028<1071:aosftt>2.0.co;2

Xie, P., & Arkin, P. A. (1997). Global precipitation: A 17-year monthly analysis based on gauge observations, satellite estimates, and numerical model outputs. *Bulletin of the American Meteorological Society*, *78*, 2539–2558. https://doi.org/10.1175/1520-0477(1997)078<2539:gpayma>2.0.co;2

Yu, L. (2011). A global relationship between the ocean water cycle and near-surface salinity. *Journal of Geophysical Research*, *116*, C10025. https://doi.org/10.1029/2010JC006937

Yu, L., & Weller, R. A. (2007). Objectively analyzed air-sea heat fluxes for the global ice-free oceans (1981-2005). *Bulletin of the American Meteorological Society*, *88*, 527–540. https://doi.org/10.1175/bams-88-4-527

Zeng, L., Du, Y., Xie, S.-P., & Wang, D. (2009). Barrier layer in the South China Sea during summer 2000. *Dynamics of Atmospheres and Oceans*, *47*(1), 38–54. https://doi.org/10.1016/j.dynatmoce.2008.08.001

Zeng, L., & Wang, D. (2017). Seasonal variations in the barrier layer in the South China Sea: Characteristics, mechanisms and impact of warming. *Climate Dynamics*, *48*(1), 1911–1930. https://doi.org/10.1007/s00382-016-3182-8

Zhang, X., & Clarke, A. J. (2015). Observations of Interannual Equatorial Freshwater Jets in the Western Pacific. *Journal of Physical Oceanography*, *45*, 2848–2865. https://doi.org/10.1175/jpo-d-14-0245.1

Zhong, W., Cai, W., Zheng, X.-T., & Yang, S. (2019). Unusual anomaly pattern of the 2015/2016 extreme El Niño induced by the 2014 warm condition. *Geophysical Research Letters*, *46*. https://doi.org/10.1029/2019gl085681